
Quantification of Cerebral Blood Flow and Oxygen Metabolism with 3-Dimensional PET and ^{15}O : Validation by Comparison with 2-Dimensional PET

Masanobu Ibaraki¹, Shuichi Miura¹, Eku Shimosegawa^{1,2}, Shigeki Sugawara¹, Tetsuro Mizuta³, Akihiro Ishikawa³, and Masaharu Amano³

¹Department of Radiology and Nuclear Medicine, Akita Research Institute of Brain and Blood Vessels, Akita, Japan; ²Department of Nuclear Medicine and Tracer Kinetics, Osaka University Graduate School of Medicine, Osaka, Japan; and ³Medical System Division, Shimadzu Corporation, Kyoto, Japan

Quantitative PET with ^{15}O provides absolute values for cerebral blood flow (CBF), cerebral blood volume (CBV), cerebral metabolic rate of oxygen (CMRO_2), and oxygen extraction fraction (OEF), which are used for assessment of brain pathophysiology. Absolute quantification relies on physically accurate measurement, which, thus far, has been achieved by 2-dimensional PET (2D PET), the current gold standard for measurement of CBF and oxygen metabolism. We investigated whether quantitative ^{15}O study with 3-dimensional PET (3D PET) shows the same degree of accuracy as 2D PET. **Methods:** 2D PET and 3D PET measurements were obtained on the same day on 8 healthy men (age, 21–24 y). 2D PET was performed using a PET scanner with bismuth germanate (BGO) detectors and a 150-mm axial field of view (FOV). For 3D PET, a 3D-only tomograph with gadolinium oxyorthosilicate (GSO) detectors and a 156-mm axial FOV was used. A hybrid scatter-correction method based on acquisition in the dual-energy window (hybrid dual-energy window [HDE] method) was applied in the 3D PET study. Each PET study included 3 sequential PET scans for C^{15}O , $^{15}\text{O}_2$, and H_2^{15}O (3-step method). The inhaled (or injected) dose for 3D PET was approximately one fourth of that for 2D PET. **Results:** In the 2D PET study, average gray matter values (mean \pm SD) of CBF, CBV, CMRO_2 , and OEF were 53 ± 12 (mL/100 mL/min), 3.6 ± 0.3 (mL/100 mL), 3.5 ± 0.5 (mL/100 mL/min), and 0.35 ± 0.06 , respectively. In the 3D PET study, scatter correction strongly affected the results. Without scatter correction, average values were 44 ± 6 (mL/100 mL/min), 5.2 ± 0.6 (mL/100 mL), 3.3 ± 0.4 (mL/100 mL/min), and 0.39 ± 0.05 , respectively. With the exception of OEF, values differed between 2D PET and 3D PET. However, average gray matter values of scatter-corrected 3D PET were comparable to those of 2D PET: 55 ± 11 (mL/100 mL/min), 3.7 ± 0.5 (mL/100 mL), 3.8 ± 0.7 (mL/100 mL/min), and 0.36 ± 0.06 , respectively. Even though the 2 PET scanners with different crystal materials, data acquisition systems, spatial

resolution, and attenuation-correction methods were used, the agreement of the results between 2D PET and scatter-corrected 3D PET was excellent. **Conclusion:** Scatter coincidence is a problem in 3D PET for quantitative ^{15}O study. The combination of both the present PET/CT device and the HDE scatter correction permits quantitative 3D PET with the same degree of accuracy as 2D PET and with a lower radiation dose. The present scanner is also applicable to conventional steady-state ^{15}O gas inhalation if inhaled doses are adjusted appropriately.

Key Words: CBF; CMRO_2 ; 3D PET with ^{15}O ; scatter correction

J Nucl Med 2008; 49:50–59

DOI: 10.2967/jnumed.107.044008

Evaluation of cerebral circulation and metabolism plays an important role in the assessment of brain pathophysiology and in decisions with regard to the therapeutic strategy for patients with brain ischemia (1–4). Quantitative PET with ^{15}O provides absolute values for cerebral blood flow (CBF), cerebral blood volume (CBV), cerebral metabolic rate of oxygen (CMRO_2), and oxygen extraction fraction (OEF) (5–7). Quantitative oxygen metabolic images cannot be obtained by other imaging modalities such as SPECT or MRI; this is a major advantage of PET with ^{15}O .

Absolute quantification of these variables relies on physically accurate PET measurement, which, thus far, has been achieved by 2-dimensional PET (2D PET) with appropriate data corrections, including randoms correction, radioactive decay correction, attenuation correction, dead-time correction, and detector normalization. In recent years, PET acquisition in the 3-dimensional (3D) mode has become popular, and 3D-only PET scanners are now commercially available (8). In contrast to conventional 2D PET scanners with inter-plane septa, 3D PET scanners acquire all possible lines of response by removing the septa, allowing for a higher sensitivity and lower radiation dose. However, scatter-coincidence

Received Jun. 5, 2007; revision accepted Oct. 9, 2007.

For correspondence or reprints contact: Masanobu Ibaraki, PhD, Department of Radiology and Nuclear Medicine, Akita Research Institute of Brain and Blood Vessels, 6-10 Senshu-Kubota Machi, Akita 010-0874, Japan.

E-mail: iba@akita-noken.go.jp

COPYRIGHT © 2008 by the Society of Nuclear Medicine, Inc.

events, which disturb the quantitative nature of PET, constitute a significant proportion of the total detected events in 3D PET. 3D PET is not generally used clinically for the quantitative brain study with ^{15}O . Although there are some reports on the validation of 3D PET (9–14), to our knowledge, no direct comparison between 3D PET and 2D PET exists for measurements of CBF, CBV, CMRO_2 , and OEF.

The aim of this study was to investigate whether ^{15}O PET with a 3D-only scanner is as reliable as 2D PET. We hypothesized that appropriate scatter correction in 3D PET makes it possible to perform ^{15}O PET with a lower radiation dose and with the same degree of accuracy as 2D PET. We performed 2D PET and 3D PET sequentially on healthy volunteers and compared the CBF, CBV, CMRO_2 , and OEF values. For 3D PET, a 3D-only scanner was used with a hybrid scatter-correction method (15,16).

MATERIALS AND METHODS

Subjects

Eight healthy men, 21- to 24-y-old, were recruited and provided written informed consent. Two sequential PET studies, with a 2D scanner and a 3D-only scanner, were performed on the same day with each subject at rest. The order of the studies (2D, 3D) was randomized. All volunteers were determined to be healthy on the basis of medical history, blood screening tests, anatomic MRI (T1- and T2-weighted images), and MR angiography of the brain. MRI was performed with a 1.5-T whole-body scanner (Magnetom Vision; Siemens Medical Solutions, Inc.). Three-dimensional T1-weighted images (magnetization-prepared rapid acquisition gradient echo [MPRAGE] sequence; repetition time, 9.7 ms; echo time, 4.0 ms; inversion time, 300 ms; flip angle, 12° ; isotropic voxel size, 1 mm) were also used as anatomic references in subsequent region-of-interest (ROI) analysis. The study protocol was approved by the Ethics Committee of the Akita Research Institute of Brain and Blood Vessels.

2D PET Scanner

2D PET was performed with a SET-2300W scanner (Shimadzu Corp.), which uses bismuth germanate (BGO) detectors and provides 47 sections with a center-to-center distance of 3.125 mm (17). The axial field of view (FOV) was 150 mm. The intrinsic spatial resolution was 4.5-mm full width at half maximum (FWHM) in-plane and 4.5-mm FWHM axially. Although the septa can be retracted for 3D acquisition, all data were acquired in 2D mode with the septa in place. The coincidence time window was set to 18 ns.

Image reconstruction with a filtered-backprojection (FBP) algorithm and a Butterworth filter resulted in a final in-plane resolution of approximately 8-mm FWHM. Slices were rebinned by adding sinograms in groups of 2 with a 1-slice overlap between adjacent groups, resulting in 46 reconstructed slices. Before the emission scans, a transmission scan (10 min) with a $^{68}\text{Ge}/^{68}\text{Ga}$ external source was performed for attenuation correction. The PET scanner was calibrated by scanning a cylindrical phantom (14 cm in diameter) filled with a ^{68}Ga aqueous solution with a known radioactivity concentration. In this procedure, an ROI of 10 cm in diameter was placed in the center of the phantom image. Detector normalization, attenuation correction, and image reconstruction were applied identically to the calibration phantom and to the subjects. No scatter correction was applied.

3D PET Scanner

For 3D PET, a SET-3000GCT/M scanner (PET/CT; Shimadzu Corp.) dedicated to the 3D mode was used (15). It uses gadolinium oxyorthosilicate (GSO) detectors and provides 59 sections with a center-to-center distance of 2.6 mm. The axial FOV was 156 mm. The intrinsic spatial resolution was 3.5-mm FWHM in-plane and 4.2-mm FWHM axially. In this study, the scanner was operated in a static scan mode with dual-energy window acquisition. The coincidence time window was set to 6 ns. To reduce the counting rate of random coincidence and scatter coincidence attributable to radioactivity outside the FOV, we used a prototype shield module consisting of 7-mm-thick lead plates attached to the gantry bed and covering the breast and shoulder of the subject.

FBP image reconstruction followed by 3D gaussian smoothing with 6-mm FWHM resulted in a final in-plane resolution of approximately 7-mm FWHM. Before the emission scans, a transmission scan (3 min) with a ^{137}Cs point source was performed with a BGO transmission detector ring coaxially attached to the GSO emission detector ring (15). The PET scanner was calibrated by scanning a cylindrical phantom (15 cm in diameter) filled with a ^{68}Ga aqueous solution with a known radioactivity concentration. In this calibration procedure, an ROI of 10-cm diameter was placed in the center of the phantom image. Detector normalization, attenuation correction, scatter correction, and image reconstruction were applied identically to the calibration phantom and to the subjects.

A hybrid scatter-correction method, based on acquisition in the dual-energy window combined with a convolution-subtraction method in the upper energy window (UEW), was used (16,18). In this article, this method is referred to as the hybrid dual-energy window (HDE) method. Coincidence events were assigned to the standard energy window (SEW) when both photons fell within the standard photopeak window (300–700 keV). Additionally, when both photons deposited energy in the range of 480–700 keV, the events were also recorded as UEW data. Raw data for each window were acquired simultaneously and then converted off-line to 2D sinograms by a Fourier rebinning algorithm (19). Therefore, subsequent data processing could be done in 2D calculation without the computational burden of 3D data manipulation.

Estimation of the true (scatter-free) component of the SEW data was performed on a sinogram basis as follows:

(i) The convolution-subtraction method was applied to the UEW data for scatter correction (20). The scatter component of the UEW data, $UEW_{scatter}$, which is thought to be quite small in comparison with that of the SEW data, was estimated by convolving a 2D scatter kernel with the 2D projection (coronal view) of the UEW sinograms. The scatter kernel was defined as a 2D low-pass filter in the spatial frequency domain, $1/(1 + \alpha \exp(\beta |\mathbf{f}|^2))$, where \mathbf{f} represents spatial frequency and α and β are optimization parameters. This function was empirically selected to represent the scatter tail of objects. We optimized the parameters (α , β) by matching the calculated scatter distribution with the measured scatter tail of cylindrical phantom (15 cm in diameter). The true (scatter-free) component of the UEW data, UEW_{true} , was calculated as:

$$UEW_{true} = UEW - UEW_{scatter}.$$

(ii) The scatter component of the SEW data, $SEW_{scatter}$, was calculated as a subtraction of UEW_{true} scaled by factor f from the SEW data as:

$$SEW_{scatter} = SEW - f \times UEW_{true}$$

The scaling factor f between the 2 energy windows was determined from the phantom data according to the manner of Ferreira et al. (18). For the current configuration of energy windows (480–700 keV for UEW, 300–700 keV for SEW) the scaling factor was approximately 2.5. The energy width of the UEW (480–700 keV) was optimized as a compromise between the number of detected events in the UEW and the accuracy of the scatter correction (convolution-subtraction method) for the UEW data.

(iii) In the final step, the true component of SEW, SEW_{true} , was estimated as a subtraction of smoothed $SEW_{scatter}$, $(SEW_{scatter})_{smoothed}$, from the SEW data as:

$$SEW_{true} = SEW - (SEW_{scatter})_{smoothed}$$

A boxcar moving average with a 50-mm square was used for smoothing. As a result, a scatter-corrected sinogram (corresponding to SEW_{true}) and an uncorrected sinogram (corresponding to SEW) were created and were cross-calibrated with cylindrical phantom data processed with and without scatter correction, respectively.

PET Procedure

Each PET study included a transmission scan for attenuation correction and 3 static emission scans with the inhalation of $C^{15}O$, the inhalation of $^{15}O_2$, and the injection of $H_2^{15}O$ (21). The interval between scans was approximately 15 min. A head fixation system was applied for each subject to minimize head movement during scanning. The subjects inhaled the gases ($C^{15}O$ and $^{15}O_2$) through a disposable plastic face mask under the condition of natural respiration. The gases were supplied at a flow rate of 500 mL/min and at a constant concentration of radioactivity. Blood gases were measured at the beginning and at the end of the scanning.

$C^{15}O$ PET studies were performed to measure CBV (22). Static PET was initiated 3 min after 1 min of continuous inhalation of $C^{15}O$ gas. Scanning lasted 4 min. The total doses of radioactivity supplied by mouth were 5.5 ± 0.7 GBq (average \pm SD; $n = 8$) for 2D PET and 1.3 ± 0.2 GBq for 3D PET. Effective dose estimates to each subject for 2D and 3D PET were 2.8 and 0.7 mSv, respectively. Three arterial blood samples were taken during scanning to measure whole-blood radioactivity. The cerebral-to-large vessel hematocrit ratio was assumed to be 0.85 (23).

$H_2^{15}O$ PET studies were performed to measure CBF. The protocol consisted of 3 min of static scanning initiated simultaneously with 2 min of intravenous infusion of $H_2^{15}O$. Injected doses at the start of scanning were 1.5 GBq for 2D PET and 0.4 GBq for 3D PET. Effective dose estimates to each subject for 2D and 3D PET were 1.4 and 0.3 mSv, respectively. An arterial input function was determined with a β -detector system that continuously measured radioactivity in arterial whole blood taken from the radial artery. Delay and dispersion occurring in the β -detector system and the internal arterial line were corrected as described previously (24,25). CBF was calculated by the autoradiographic method (7,26,27).

$^{15}O_2$ PET studies were performed to measure OEF and $CMRO_2$ (6). The protocol consisted of 3 min of static scanning initiated simultaneously with 1.5 min of inhalation of $^{15}O_2$. The total doses of radioactivity supplied by mouth were 12.2 ± 0.5 GBq for 2D

PET and 3.0 ± 0.3 GBq for 3D PET. Effective dose estimates to each subject for 2D and 3D PET were 4.7 and 1.2 mSv, respectively. The arterial input function was determined in the same way as that for the $H_2^{15}O$ PET scan. The contribution of ^{15}O -labeled metabolic water was estimated according to the method of Iida et al. (28).

Data Analysis

For each subject, 3 sets of parametric maps (CBF, CBV, $CMRO_2$, and OEF) were produced for 2D PET, uncorrected 3D PET, and scatter-corrected 3D PET. The 3D PET maps were registered with 2D PET maps with SPM99 (Wellcome Department of Cognitive Neurology) (29,30). All PET maps (2D and 3D) were then transformed to standard brain size and shape with linear and nonlinear parameters with SPM99 and a built-in CBF template. Thus, the resultant parametric maps of all subjects had the same anatomic format with an isotropic voxel size of 2 mm. The ROIs defined in the study by Ito et al. (31) were subsequently applied for all parametric maps. The individual T1-weighted image was examined to confirm the proper arrangement of the ROIs.

Circular ROIs 16 mm in diameter were defined for the pons, midbrain, thalamus, putamen, parahippocampal gyrus, and anterior and posterior parts of the cingulate gyrus, and elliptic ROIs of 16×32 mm were defined for the cerebellar cortex, centrum semiovale, and 4 neocortical regions representing the frontal, temporal, occipital, and parietal lobes. ROIs were drawn bilaterally for each brain region (if possible) in 3 adjacent slices, and data were averaged. Mean values and SD for CBF, CBV, $CMRO_2$, and OEF were calculated for 8 subjects. Differences in each variable between 2D PET, uncorrected 3D PET, and scatter-corrected 3D PET were examined by a paired t test with Bonferroni correction for multiple comparisons. Significance was accepted at $P < 0.05$. Correlation analysis between 2D PET and 3D PET was performed to examine the deviation from the line of identity. Regression lines were determined by principal component analysis. Bland-Altman analysis was also performed to confirm the agreement between 2D PET and scatter-corrected 3D PET (32).

RESULTS

Blood Gas Analysis

The $Paco_2$ (partial pressure of carbon dioxide, arterial), PaO_2 (partial pressure of oxygen, arterial), pH, blood pressure, and heart rate during each scanning are summarized in Table 1. The $Paco_2$ ($P = 0.03$) and pH ($P = 0.04$) during the $H_2^{15}O$ scanning differed statistically between 2D PET and the 3D PET, but the differences were marginal (1.3 mm Hg and <0.01 , respectively). In other items, no significant difference was observed. The arterial hemoglobin concentration and hematocrit during these studies (mean \pm SD.) were 14.7 ± 1.0 g/dL and $45.0\% \pm 3.0\%$, respectively.

PET

Representative images of 3D PET for $^{15}O_2$, $C^{15}O$, and $H_2^{15}O$ are shown in Figure 1. The random counting rate was much higher in $^{15}O_2$ PET compared with $C^{15}O$ and $H_2^{15}O$ PET primarily because of the high concentration of radioactivity in the gas mask (outside the FOV) and in the upper airway. During $^{15}O_2$ PET, the coincidence counting rate reached up to 300 kcps (1,300-kcps prompt and 1,000-kcps

TABLE 1
Paco₂, Pao₂, pH, Blood Pressure (BP), and Heart Rate (HR) During 2D and 3D PET (*n* = 8)

Scanning	Mode	Paco ₂ (mm Hg)	Pao ₂ (mm Hg)	pH	BP _{Systolic} (mm Hg)	BP _{Diastolic} (mm Hg)	HR (beats/min)
H ₂ ¹⁵ O	2D	41.5 ± 3.0	94.3 ± 9.3	7.395 ± 0.018	135.7 ± 12.8	65.3 ± 10.1	63 ± 10
	3D	40.2 ± 2.2*	98.7 ± 7.1	7.402 ± 0.015*	134.6 ± 13.4	66.4 ± 9.9	64 ± 13
C ¹⁵ O	2D	39.1 ± 2.8	99.1 ± 9.1	7.406 ± 0.020	132.8 ± 15.4	64.6 ± 7.2	64 ± 12
	3D	38.7 ± 1.9	105.3 ± 9.8	7.413 ± 0.012	135.9 ± 12.3	65.0 ± 9.6	61 ± 12
¹⁵ O ₂	2D	41.0 ± 2.9	95.1 ± 10.7	7.388 ± 0.019	133.3 ± 12.9	63.6 ± 7.3	64 ± 12
	3D	41.0 ± 3.2	95.4 ± 8.9	7.391 ± 0.020	135.5 ± 13.6	65.7 ± 10.1	60 ± 12

*Significant difference from 2D PET value (paired *t* test, *P* < 0.05).
Values are shown as mean ± SD.

random counting rate) with 3D PET and 100 kcps (550-kcps prompt and 450-kcps random counting rate) with 2D PET. During C¹⁵O PET, maximum counting rates, which occurred at the start of scanning, were 50 kcps (70-kcps prompt and 20-kcps random counting rate) with 3D PET and 20 kcps (30-kcps prompt and 10-kcps random counting rate) with 2D PET. During H₂¹⁵O PET, the coincidence counting rate reached up to 300 kcps (450-kcps prompt and 150-kcps random counting rate) with 3D PET and 100 kcps (200-kcps prompt and 100-kcps random counting rate) with 2D PET. Despite the lower radioactivity dose in 3D PET, the maximum counting rate was approximately 3 times that of 2D PET, reflecting the higher sensitivity and better counting rate performance of the 3D PET scanner.

CBF

CBF, CBV, CMRO₂, and OEF values for 13 brain regions are given in Table 2. Gray-to-white matter ratios of these

variables are also included. Anatomically standardized maps for a subject (subject 4) are shown in Figure 2.

In 8 of 13 brain regions, statistically significant differences in CBF between 2D PET and uncorrected 3D PET were observed (Table 2). Compared with 2D PET, uncorrected 3D PET gave larger CBF values in the centrum semiovale and smaller values in the gray matter brain regions, resulting in lower gray-to-white matter CBF ratios. No statistically significant differences in CBF were observed between 2D PET and corrected 3D PET. Corrected 3D PET resulted in gray-to-white matter ratios close to those of 2D PET and showed similar image contrast (Fig. 2).

CBV

In all brain regions, the CBV values were significantly larger with uncorrected 3D PET than with 2D PET (Table 2). In contrast, no statistically significant difference was observed between 2D PET and corrected 3D PET for any

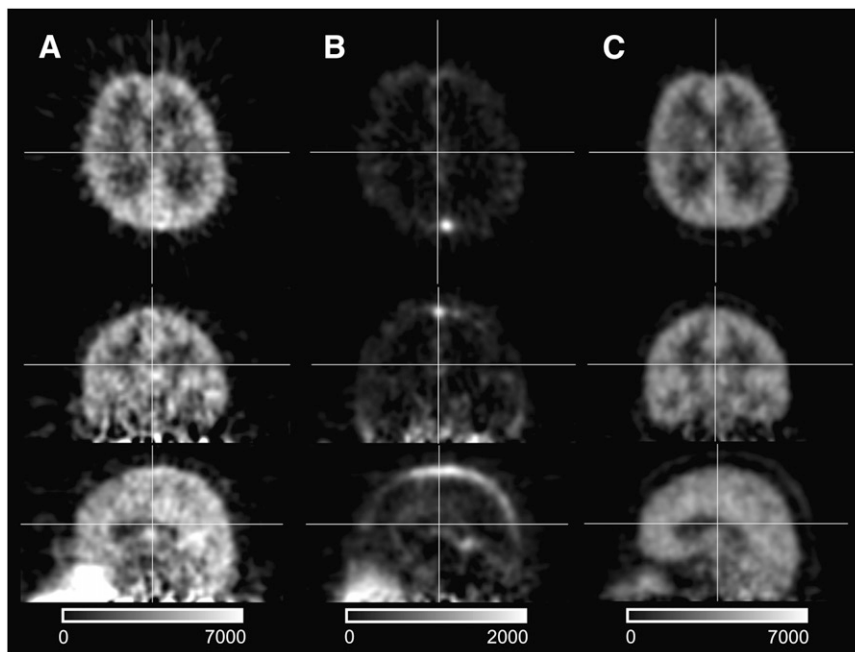


FIGURE 1. Representative images (subject 1) of 3D PET for ¹⁵O₂ (A), C¹⁵O (B), and H₂¹⁵O (C) in axial view (top), coronal view (middle), and sagittal view (bottom). Images were scatter-corrected by the HDE method. ¹⁵O₂ image shows high concentration of radioactivity in upper airway because of acquisition during inhalation of ¹⁵O₂ gases.

TABLE 2
Average CBF, CBV, CMRO₂, and OEF Values (*n* = 8)

Parameter	CBF (mL/100 mL/min)			CBV (mL/100 mL)		
	Scan mode	3D PET		2D PET	3D PET	
		Scatter correction	No		HDE	No
Pons	45 ± 10	44 ± 8	46 ± 11	3.0 ± 0.9	5.8 ± 1.1*	3.4 ± 1.0†
Cerebellum	59 ± 14	50 ± 9*	68 ± 21†	4.0 ± 0.7	5.6 ± 0.8*	3.9 ± 1.1†
Parahippocampal gyrus	44 ± 9	43 ± 6	47 ± 8	5.0 ± 0.6	6.6 ± 1.0*	4.8 ± 0.9†
Midbrain	44 ± 7	43 ± 6	45 ± 8	3.2 ± 0.6	6.0 ± 0.8*	3.7 ± 0.8†
Putamen	64 ± 22	51 ± 8	64 ± 13†	2.7 ± 0.7	5.0 ± 0.6*	2.9 ± 0.4†
Temporal cortex	52 ± 12	40 ± 6*	51 ± 9†	3.7 ± 0.5	4.7 ± 0.5*	3.6 ± 0.4†
Frontal cortex	50 ± 10	37 ± 4*	50 ± 8†	3.4 ± 0.3	4.0 ± 0.6*	3.1 ± 0.6†
Anterior cingulate	56 ± 17	41 ± 8*	57 ± 17†	3.8 ± 0.6	4.8 ± 0.5*	3.7 ± 0.6†
Thalamus	56 ± 14	50 ± 7	59 ± 11†	3.3 ± 0.5	5.5 ± 0.7*	3.4 ± 0.5†
Occipital cortex	58 ± 15	45 ± 7*	58 ± 11†	4.5 ± 0.5	5.7 ± 0.9*	4.7 ± 0.7†
Posterior cingulate	58 ± 15	48 ± 7*	61 ± 13†	3.8 ± 0.4	5.0 ± 0.4*	3.6 ± 0.6†
Parietal cortex	49 ± 7	38 ± 5*	51 ± 10†	3.3 ± 0.4	4.1 ± 0.5*	3.2 ± 0.3†
Centrum semiovale	19 ± 3	23 ± 2*	20 ± 2†	1.7 ± 0.3	3.7 ± 0.5*	1.8 ± 0.4†
Gray matter total	53 ± 12	44 ± 6*	55 ± 11†	3.6 ± 0.3	5.2 ± 0.6*	3.7 ± 0.5†
Gray-to-white matter ratio	2.8 ± 0.3	1.9 ± 0.2*	2.7 ± 0.4†	2.2 ± 0.3	1.4 ± 0.1*	2.1 ± 0.3†

Parameter	CMRO ₂ (mL/100 mL/min)			OEF		
	Scan mode	3D PET		2D PET	3D PET	
		Scatter correction	No		HDE	No
Pons	2.7 ± 0.5	3.1 ± 0.5*	2.7 ± 0.6	0.31 ± 0.05	0.36 ± 0.06*	0.31 ± 0.07†
Cerebellum	3.8 ± 0.7	3.5 ± 0.4	4.4 ± 1.1†	0.34 ± 0.06	0.37 ± 0.06	0.35 ± 0.07†
Parahippocampal gyrus	2.3 ± 0.3	3.1 ± 0.4*	2.9 ± 0.5*	0.28 ± 0.05	0.37 ± 0.04*	0.32 ± 0.05†
Midbrain	2.8 ± 0.5	3.4 ± 0.3*	3.1 ± 0.4†	0.33 ± 0.06	0.41 ± 0.05*	0.37 ± 0.06*†
Putamen	4.7 ± 0.9	4.1 ± 0.7	4.9 ± 1.1†	0.40 ± 0.09	0.42 ± 0.08	0.40 ± 0.09
Temporal cortex	3.7 ± 0.5	3.2 ± 0.4*	3.9 ± 0.6†	0.38 ± 0.07	0.42 ± 0.07	0.40 ± 0.07†
Frontal cortex	3.3 ± 0.5	2.7 ± 0.4*	3.4 ± 0.6†	0.35 ± 0.05	0.39 ± 0.05*	0.35 ± 0.06†
Anterior cingulate	3.5 ± 0.8	2.9 ± 0.5*	3.5 ± 0.9†	0.34 ± 0.07	0.37 ± 0.06*	0.33 ± 0.06†
Thalamus	3.7 ± 0.5	3.5 ± 0.5	3.8 ± 0.8	0.36 ± 0.06	0.37 ± 0.05	0.34 ± 0.05†
Occipital cortex	4.3 ± 0.8	3.5 ± 0.3*	4.3 ± 0.7†	0.40 ± 0.06	0.40 ± 0.05	0.39 ± 0.05
Posterior cingulate	4.0 ± 0.6	3.6 ± 0.6*	4.4 ± 0.9†	0.37 ± 0.07	0.39 ± 0.06	0.38 ± 0.07
Parietal cortex	3.7 ± 0.5	3.0 ± 0.4*	3.9 ± 0.8†	0.39 ± 0.06	0.40 ± 0.05	0.40 ± 0.05
Centrum semiovale	1.4 ± 0.2	1.7 ± 0.2*	1.5 ± 0.3†	0.41 ± 0.08	0.40 ± 0.06	0.39 ± 0.09
Gray matter total	3.5 ± 0.5	3.3 ± 0.4	3.8 ± 0.7†	0.35 ± 0.06	0.39 ± 0.05*	0.36 ± 0.06†
Gray-to-white matter ratio	2.5 ± 0.2	1.9 ± 0.2*	2.6 ± 0.5†	0.87 ± 0.04	0.98 ± 0.07*	0.94 ± 0.10

*Significant difference vs. 2D PET value.

†Significant difference vs. uncorrected 3D PET value.

Gray matter total = values averaged over 12 gray matter regions; Gray-to-white matter ratio = ratio of gray matter total to white matter value of the centrum semiovale.

Values are shown as mean ± SD. Differences between studies were examined by paired *t* test (*P* < 0.05) with Bonferroni correction for multiple comparisons.

brain region. Corrected 3D PET resulted in gray-to-white matter ratios close to those of 2D PET and showed similar image contrast (Fig. 2).

CMRO₂

In 10 of 13 brain regions, statistically significant differences in CMRO₂ between 2D PET and uncorrected 3D PET were observed (Table 2). Although the trend was similar to that of CBF, CMRO₂ values in the pons, parahippocampal gyrus, and midbrain were larger with uncorrected 3D PET

than with 2D PET—opposite to the CBF results. In almost all regions (12/13), CMRO₂ values were not statistically different between 2D PET and corrected 3D PET. Corrected 3D PET resulted in gray-to-white matter ratios close to those of 2D PET and showed similar image contrast (Fig. 2).

OEF

In contrast to CBF, CBV, and CMRO₂, differences in OEF were not large between PET studies. In 5 of 13 brain regions, statistically significant differences in OEF between

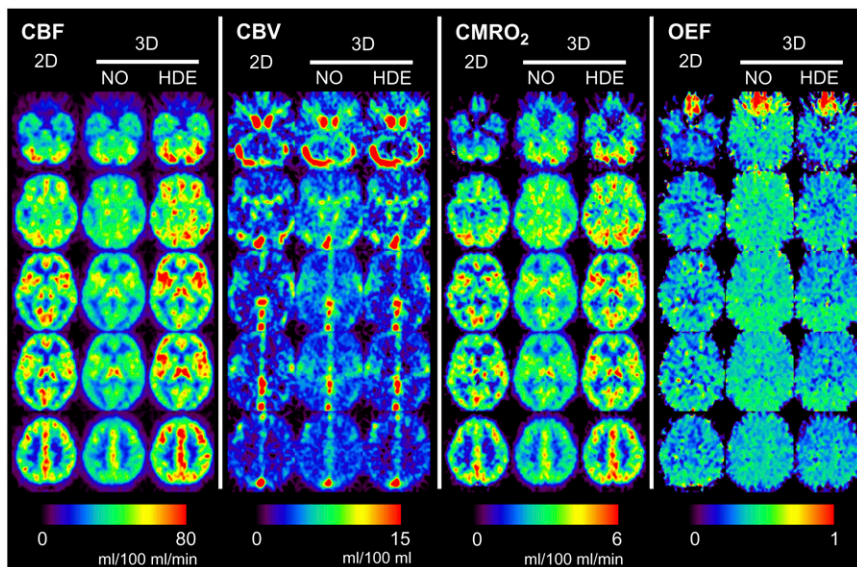


FIGURE 2. Anatomically standardized CBF, CBV, $CMRO_2$, and OEF images of a single subject (subject 4) obtained with 2D PET (left), uncorrected 3D PET (middle), and scatter-corrected 3D PET by the HDE method (right). Slice positions are -36 , -18 , 0 , 6 , and 36 mm from anterior commissure–posterior commissure line.

2D PET and uncorrected 3D PET were observed (Table 2). A difference between 2D PET and corrected 3D PET was observed only in the midbrain.

Graphic Analysis

Figures 3 and 4 show the scatter plots correlating 2D PET with uncorrected 3D PET and scatter-corrected 3D PET, respectively. Coefficients of correlation and linear regression

lines are also shown. For CBF, $CMRO_2$, and OEF, good correlations were obtained, irrespective of 3D PET scatter correction, although the coefficients were slightly larger when scatter correction was applied. For CBV, scatter correction improved the correlation substantially (0.519 without correction, 0.710 with correction). For all variables, the regression line was closer to the line of identity for corrected 3D PET than that for uncorrected 3D PET.

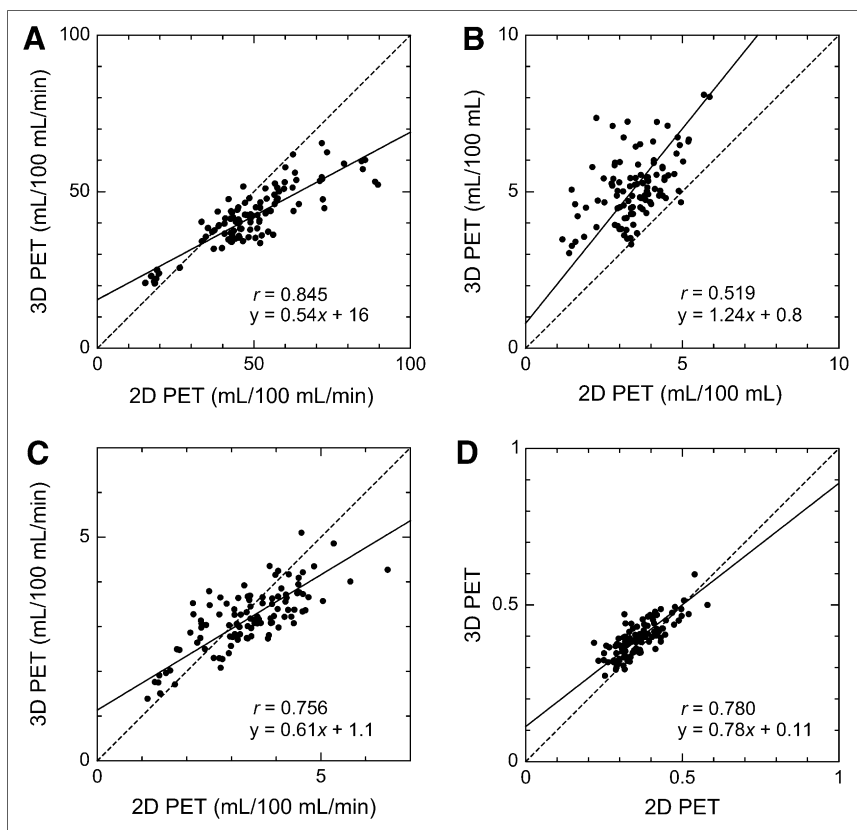


FIGURE 3. Correlation between 2D PET and uncorrected 3D PET for CBF (A), CBV (B), $CMRO_2$ (C), and OEF (D). Number of data points is 104 (8 subjects \times 13 ROIs) for each dataset. Regression line, determined by principal component analysis (solid line), and line of identity (dashed line) are also shown.

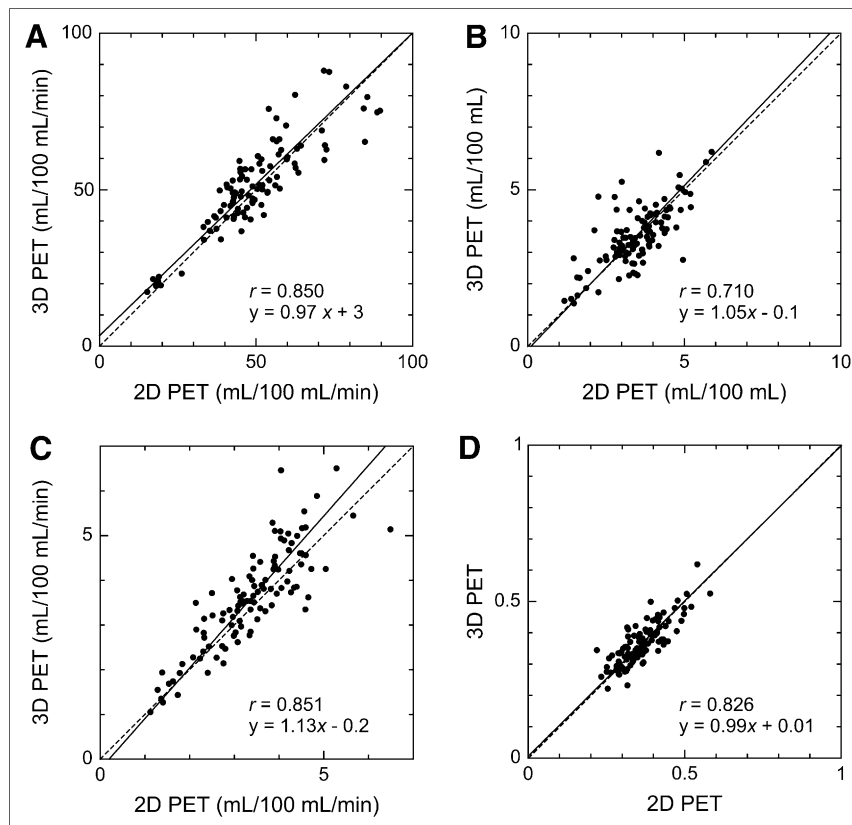


FIGURE 4. Correlation between 2D PET and scatter-corrected 3D PET for CBF (A), CBV (B), CMRO₂ (C), and OEF (D). Number of data points is 104 (8 subjects × 13 ROIs) for each dataset. Regression line, determined by principal component analysis (solid line), and line of identity (dashed line) are also shown.

The Bland–Altman plot of the difference in each variable between 2D PET and scatter-corrected 3D PET against their mean value is shown in Figure 5. Although there was a trend toward larger fluctuation for higher CBF and CMRO₂, no systematic bias was observed over the range of measurement for all variables. The mean differences (2D PET – scatter-corrected 3D PET) in CBF, CBV, CMRO₂, and OEF were -2 ± 9 (mL/100 mL/min), 0.0 ± 0.7 (mL/100 mL), -0.2 ± 0.6 (mL/100 mL/min), and 0.00 ± 0.04 , respectively.

DISCUSSION

To validate the use of 3D PET with ¹⁵O for quantitative measurement of cerebral circulation and oxygen metabolism, we performed a comparative study with 2D PET, the gold standard. A 3D-only GSO scanner with a high counting-rate performance, achieved with a short coincidence time window (6 ns) and advanced electronic circuits, was used (15). The present results showed clear differences in CBF, CBV, and CMRO₂ values between uncorrected 3D PET and 2D PET. Decreased image contrast was observed with uncorrected 3D PET. Application of HDE scatter correction resulted in CBF, CBV, CMRO₂, and OEF values and their gray-to-white matter ratios similar to those obtained with 2D PET.

This study used 2 PET scanners with different crystal materials, data acquisition systems, spatial resolution, and

attenuation-correction methods. From a viewpoint of validation of scatter correction in 3D PET, this is a limitation of the study. The present 3D scanner uses the single photon ¹³⁷Cs point source for transmission scanning rather than the conventional ⁶⁸Ge/⁶⁸Ga coincidence method as used in the 2D scanner (15). Because of the different energy (662 keV) of the ¹³⁷Cs γ -ray, measured attenuation coefficients were converted to those for 511 keV by simple multiplication with a constant factor (33). Although the ¹³⁷Cs transmission scanning is considered to be a reliable method, at least for uniform structures such as brain, the effect of the transmission scanning needs to be evaluated quantitatively. We did not apply scatter correction in 2D PET, but the scatter fraction of the 2D scanner was relatively small, approximately 10% (17,34), which may decrease the gray-to-white matter ratio of CBF and CMRO₂ by 5%–10% according to our phantom examinations. Even though these methodologic differences existed, the agreement of the results between 2D PET and scatter-corrected 3D PET was excellent, showing that the present PET/CT device substitutes for the current 2D scanner.

The scatter-correction method used for 3D PET was the HDE method (16,18), which is based on simultaneous PET acquisition with a dual-energy window, the SEW in the 300- to 700-keV range, and the UEW in the 480- to 700-keV range. Various correction methods, including the convolution-subtraction method, the simulation-based

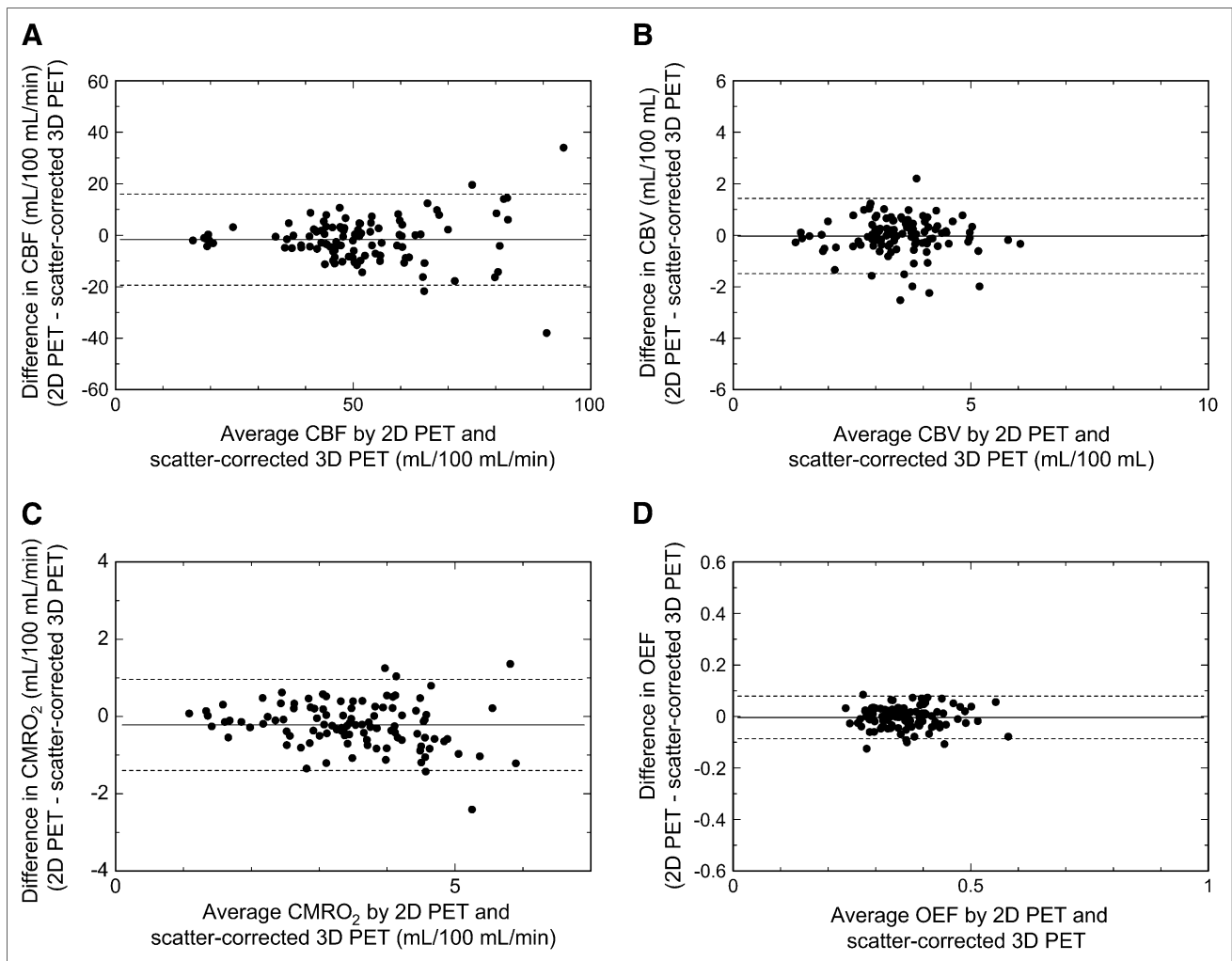


FIGURE 5. Bland–Altman plot (difference against mean) with 2D PET and scatter-corrected 3D PET for CBF (A), CBV (B), CMRO₂ (C), and OEF (D). Mean difference (solid line) and ± 2 SD (dashed line) are shown.

method, the reconstruction-based method, and their variants, have been proposed (35,36). These methods assume that radioactivity exists only inside the FOV for the estimation of scatter distribution. In contrast, the HDE method involves no such assumption because the scatter distribution is estimated from the energy information of each coincidence event. The HDE method is advantageous for situations in which radioactivity exists outside the FOV, as in the ¹⁵O PET study.

The effect of radioactivity outside the FOV was expected to be greatest for the ¹⁵O₂ study because of the existence of high radioactivity in the gas inhalation mask and the lung field. In the present study, uncorrected 3D PET overestimated CMRO₂ values for lower brain regions (pons, parahippocampal gyrus, midbrain) compared with 2D PET (Table 2). This differed from the CBF results and may be due to scatter coincidence originating outside the FOV. For CMRO₂, HDE scatter correction provided absolute values close to those of 2D PET, indicating the validity of the HDE method in situations in which radioactivity exists outside the FOV.

One drawback of the scatter correction is the increased noise of the resultant image, although sinogram smoothing is applied for noise reduction. HDE scatter correction applied to 3D PET slightly increased the interindividual variability of CBF, CBV, CMRO₂, and OEF values, but the magnitudes remained comparable to those obtained with 2D PET (Table 2). The stability of the method is also important. Because the HDE method is based on simultaneous dual-energy window acquisition, the requirement for stability of the detector system and the electronic circuits is greater than that for conventional PET scanners (18). To validate the use of the HDE method in routine clinical practice, the reproducibility of CBF, CBV, CMRO₂, and OEF measurements should be confirmed. We are planning an additional study on short- and long-term reproducibility.

The present PET/CT device places the CT gantry behind the PET gantry, unlike the standard geometry. When applying the standard PET/CT scanners to the ¹⁵O brain study, we may encounter technical difficulties with regard to the treatment of the gas inhalation mask and the arterial blood

sampling. In addition, the HDE scatter correction requires the capability to acquire the coincidence events with the dual-energy (or multienergy) window mode. It must be noted that the combination of the present PET/CT device and the HDE scatter correction was essential to obtain the present results.

Instead of the conventional steady-state method with the continuous inhalation of ^{15}O -labeled gases, our group has used the 3-step method (6,21), which permits a shorter scan duration (3-min scanning for $^{15}\text{O}_2$ and H_2^{15}O) and provides a higher image contrast (gray-to-white matter ratio) with less underestimation of CBF and CMRO_2 because of the tissue mixture effect. In our experience, the present 3D scanner and the HDE scatter correction are applicable to the steady-state ^{15}O gas inhalation, in which the radioactivity is delivered at a rate of 140 MBq/min (one fourth of that for the conventional 2D steady-state measurement). The typical counting rate of $^{15}\text{O}_2$ steady-state measurement with the present 3D scanner was 50 kcps (70-kcps prompt and 20-kcps random counting rate). Although this counting rate was much lower than that with the 3-step method, image quality was comparable to that of the 3-step method because of the longer scan duration (10-min acquisition) and the lower random counting rate.

CONCLUSION

Scatter coincidence is an essential problem in quantitative 3D PET. Application of the HDE scatter-correction method with an advanced 3D PET scanner makes it possible to perform quantitative brain ^{15}O PET with the same degree of accuracy as that in 2D PET. Three-dimensional acquisition is feasible and involves a lower radiation dose than 2D PET.

ACKNOWLEDGMENTS

We thank the technical staff of the Akita Research Institute of Brain and Blood Vessels for performing the PET experiments. This research was supported by a grant from the Akita Research Institute of Brain and Blood Vessels and a Grant-in-Aid for Young Scientists (grant 18790923) from the Ministry of Education, Culture, Sports, Science and Technology of Japan.

REFERENCES

- Gibbs JM, Wise RJ, Leenders KL, Jones T. Evaluation of cerebral perfusion reserve in patients with carotid-artery occlusion. *Lancet*. 1984;1:310-314.
- Powers WJ, Grubb RL Jr, Raichle ME. Physiological responses to focal cerebral ischemia in humans. *Ann Neurol*. 1984;16:546-552.
- Sette G, Baron JC, Mazoyer B, Levasseur M, Pappata S, Crouzel C. Local brain haemodynamics and oxygen metabolism in cerebrovascular disease: positron emission tomography. *Brain*. 1989;112:931-951.
- Yamauchi H, Fukuyama H, Nagahama Y, et al. Significance of increased oxygen extraction fraction in five-year prognosis of major cerebral arterial occlusive diseases. *J Nucl Med*. 1999;40:1992-1998.
- Frackowiak RS, Lenzi GL, Jones T, Heather JD. Quantitative measurement of regional cerebral blood flow and oxygen metabolism in man using ^{15}O and positron emission tomography: theory, procedure, and normal values. *J Comput Assist Tomogr*. 1980;4:727-736.

- Mintun MA, Raichle ME, Martin WR, Herscovitch P. Brain oxygen utilization measured with O-15 radiotracers and positron emission tomography. *J Nucl Med*. 1984;25:177-187.
- Raichle ME, Martin WR, Herscovitch P, Mintun MA, Markham J. Brain blood flow measured with intravenous H_2^{15}O . II. Implementation and validation. *J Nucl Med*. 1983;24:790-798.
- Tsukamoto E, Ochi S. PET/CT today: system and its impact on cancer diagnosis. *Ann Nucl Med*. 2006;20:255-267.
- Schafers KP, Spinks TJ, Camici PG, et al. Absolute quantification of myocardial blood flow with H_2^{15}O and 3-dimensional PET: an experimental validation. *J Nucl Med*. 2002;43:1031-1040.
- Votaw JR, White M. Comparison of 2-dimensional and 3-dimensional cardiac ^{82}Rb PET studies. *J Nucl Med*. 2001;42:701-706.
- Knesaurek K, Machac J, Krynyckiy BR, Almeida OD. Comparison of 2-dimensional and 3-dimensional ^{82}Rb myocardial perfusion PET imaging. *J Nucl Med*. 2003;44:1350-1356.
- Roelants V, Bol A, Bernard X, et al. Direct comparison between 2-dimensional and 3-dimensional PET acquisition modes for myocardial blood flow absolute quantification with O-15 water and N-13 ammonia. *J Nucl Cardiol*. 2006;13:220-224.
- Dhawan V, Kazumata K, Robeson W, et al. Quantitative brain PET: comparison of 2D and 3D acquisitions on the GE Advance scanner. *Clin Positron Imaging*. 1998;1:135-144.
- Sossi V, Oakes TR, Chan GL, Schulzer M, Ruth TJ. Quantitative comparison of three- and two-dimensional PET with human brain studies. *J Nucl Med*. 1998;39:1714-1719.
- Matsumoto K, Kitamura K, Mizuta T, et al. Performance characteristics of a new 3-dimensional continuous-emission and spiral-transmission high-sensitivity and high-resolution PET camera evaluated with the NEMA NU 2-2001 standard. *J Nucl Med*. 2006;47:83-90.
- Ishikawa A, Kitamura K, Mizuta T, et al. Implementation of on-the-fly scatter correction using dual energy window method in continuous 3D whole body PET scanning. Paper presented at: IEEE Nuclear Science Symposium & Medical Imaging Conference; October 23-29, 2005; San Juan, Puerto Rico: IEEE (The Institute of Electrical and Electronics Engineers, Inc.), Piscataway, NJ; 2005: M11-138.
- Iida H, Miura S, Kanno I, Ogawa T, Uemura K. A new PET camera for noninvasive quantitation of physiological functional parametric images: Head-tome-V-dual. In: Myers R, Cunningham V, Bailey D, Jones T, eds. *Quantification of Brain Function Using PET*. San Diego, CA: Academic Press; 1996:57-61.
- Ferreira NC, Trebossen R, Lartizien C, Brulon V, Merceron P, Bendriem B. A hybrid scatter correction for 3D PET based on an estimation of the distribution of unscattered coincidences: implementation on the ECAT EXACT HR+. *Phys Med Biol*. 2002;47:1555-1571.
- Defrise M, Kinahan PE, Townsend DW, Michel C, Sibomana M, Newport DF. Exact and approximate rebinning algorithms for 3-D PET data. *IEEE Trans Med Imaging*. 1997;16:145-158.
- Bailey DL, Meikle SR. A convolution-subtraction scatter correction method for 3D PET. *Phys Med Biol*. 1994;39:411-424.
- Hatazawa J, Fujita H, Kanno I, et al. Regional cerebral blood flow, blood volume, oxygen extraction fraction, and oxygen utilization rate in normal volunteers measured by the autoradiographic technique and the single breath inhalation method. *Ann Nucl Med*. 1995;9:15-21.
- Martin WR, Powers WJ, Raichle ME. Cerebral blood volume measured with inhaled C^{15}O and positron emission tomography. *J Cereb Blood Flow Metab*. 1987;7:421-426.
- Phelps ME, Huang SC, Hoffman EJ, Kuhl DE. Validation of tomographic measurement of cerebral blood volume with C-11-labeled carboxyhemoglobin. *J Nucl Med*. 1979;20:328-334.
- Iida H, Kanno I, Miura S, Murakami M, Takahashi K, Uemura K. Error analysis of a quantitative cerebral blood flow measurement using H_2^{15}O autoradiography and positron emission tomography, with respect to the dispersion of the input function. *J Cereb Blood Flow Metab*. 1986;6:536-545.
- Iida H, Higano S, Tomura N, et al. Evaluation of regional differences of tracer appearance time in cerebral tissues using [^{15}O]water and dynamic positron emission tomography. *J Cereb Blood Flow Metab*. 1988;8:285-288.
- Iida H, Miura S, Shoji Y, et al. Noninvasive quantitation of cerebral blood flow using oxygen-15-water and a dual-PET system. *J Nucl Med*. 1998;39:1789-1798.
- Kanno I, Iida H, Miura S, et al. A system for cerebral blood flow measurement using an H_2^{15}O autoradiographic method and positron emission tomography. *J Cereb Blood Flow Metab*. 1987;7:143-153.
- Iida H, Jones T, Miura S. Modeling approach to eliminate the need to separate arterial plasma in oxygen-15 inhalation positron emission tomography. *J Nucl Med*. 1993;34:1333-1340.
- Ashburner J, Friston K. Multimodal image coregistration and partitioning: a unified framework. *Neuroimage*. 1997;6:209-217.

30. Ashburner J, Friston KJ. Nonlinear spatial normalization using basis functions. *Hum Brain Mapp.* 1999;7:254–266.
31. Ito H, Inoue K, Goto R, et al. Database of normal human cerebral blood flow measured by SPECT. I. Comparison between I-123-IMP, Tc-99m-HMPAO, and Tc-99m-ECD as referred with O-15 labeled water PET and voxel-based morphometry. *Ann Nucl Med.* 2006;20:131–138.
32. Bland JM, Altman DG. Statistical methods for assessing agreement between two methods of clinical measurement. *Lancet.* 1986;1:307–310.
33. Yu SK, Nahmias C. Single-photon transmission measurements in positron tomography using ^{137}Cs . *Phys Med Biol.* 1995;40:1255–1266.
34. Fujiwara T, Watanuki S, Yamamoto S, et al. Performance evaluation of a large axial field-of-view PET scanner: SET-2400W. *Ann Nucl Med.* 1997;11:307–313.
35. Zaidi H. Comparative evaluation of scatter correction techniques in 3D positron emission tomography. *Eur J Nucl Med.* 2000;27:1813–1826.
36. Zaidi H, Koral KF. Scatter modelling and compensation in emission tomography. *Eur J Nucl Med Mol Imaging.* 2004;31:761–782.